Research Article

A. M. Castorena-Sánchez, C. A. Velázquez-Carriles, M. A. López-Álvarez, J. C. Serrano-Niño, A. Cavazos-Garduño, L. E. Garay-Martínez, and J. M. Silva-Jara*

Magnesium nanohydroxide (2D brucite) as a host matrix for thymol and carvacrol: Synthesis, characterization, and inhibition of foodborne pathogens

https://doi.org/10.1515/gps-2023-0145
received August 5, 2023; accepted December 4, 2023

Abstract: Terpenes, such as thymol and carvacrol, are phenols that exhibit antioxidant and antimicrobial activities but are unstable in the presence of light or oxygen. Layered hydroxide salts are laminar compounds that can host molecules in their interlaminar space, protecting them from degradation and delivering bioactive molecules in a sustained manner. In the present study, hybrids composed of brucite, thymol, or carvacrol were synthesized by precipitation and anion-exchange process. The structure was confirmed by X-ray diffraction, and characteristic hexagonal morphology was verified by scanning electronic microscopy. The antibacterial activity of hybrids was evaluated against foodborne pathogens (*Escherichia coli*, *Salmonella* Enteritidis, *Listeria monocytogenes,* and *Staphylococcus aureus*), obtaining an inhibition of 80% for both Gram-positive and -negative bacteria, while inhibition of 2,2′-azino-bis(3-ethylbenzothiazoline-6-sulfonic acid) was 65% for carvacrol and 93% for thymol. Finally, the exposition of hybrids to *Artemia salina* proved to be non-toxic up to 200 $mg{\cdot}mL^{-1}$. The results suggest that these hybrids can control pathogen growth and exhibit antioxidant activity without threatening consumers' health in the case of consumption, which helps develop novel and safe products applied in the food industry.

Keywords: layered compounds, terpenes, antimicrobial activity, antioxidant activity, toxicity

1 Introduction

Foodborne illnesses constitute a significant health problem worldwide; in 2015, the World Health Organization estimated that every year in the Americas Region, 77 million people were sick, and more than 9,000 died from foodborne illness [1]. Among the foodborne disease-causing organisms identified, *Campylobacter*, pathogenic *Escherichia coli*, *Salmonella* spp., *Listeria monocytogenes*, *Staphylococcus aureus*, *Clostridium botulinum*, *Clostridium perfringens*, *Shigella*, *Vibrio*, and *Yersinia enterocolitica* are the most common foodborne pathogens associated with foods such as red meat, fish and shellfish, bivalves, dairy products, poultry, fruits, and vegetables [2–4]. For this reason, in the food industry, a set of chemical and physical treatments are carried out to eliminate, reduce, or control the presence of pathogenic microorganisms in food. The control of etiological agents by applying physical conservation methods includes heat treatments and ultraviolet radiation, ionizing radiation, high pressure, and pulsed electric fields [5]. Chemical methods include the use of antimicrobial substances that inhibit microbial growth by acting on specific targets such as the cell membrane, enzymes, and the genetic material of bacteria [6].

An example of chemical methods is the use of bioactive compounds such as carvacrol and thymol, which are monoterpenes found in the essential oils extracted from plants belonging to the *Lamiaceae* family of the genera

* **Corresponding author: J. M. Silva-Jara,** Centro Universitario de Ciencias Exactas e Ingenierías, Universidad de Guadalajara, Boulevard Marcelino García Barragán 1421, Olímpica, 44430, Guadalajara, Jalisco, México, e-mail: jorge.silva@academicos.udg.mx

A. M. Castorena-Sánchez, M. A. López-Álvarez, J. C. Serrano-Niño, A. Cavazos-Garduño, L. E. Garay-Martínez: Centro Universitario de Ciencias Exactas e Ingenierías, Universidad de Guadalajara, Boulevard Marcelino García Barragán 1421, Olímpica, 44430, Guadalajara, Jalisco, México

C. A. Velázquez-Carriles: Centro Universitario de Ciencias Exactas e Ingenierías, Universidad de Guadalajara, Boulevard Marcelino García Barragán 1421, Olímpica, 44430, Guadalajara, Jalisco, México; Centro Universitario de Tlajomulco, Universidad de Guadalajara, Carretera Tlajomulco, Santa Fé, Km 3.5, 595, CP 45641, Tlajomulco de Zúñiga, Jalisco, México.

Origanum, *Thymus*, *Coridothymus*, *Thymbra*, *Satureja*, and *Lippia*. Both substances inhibit the proliferation of Gram-positive and Gram-negative bacteria since they can damage their outer membranes. In addition, given the hydrophobic nature of thymol and carvacrol, they can integrate into bacterial cell membranes, causing disruption and alteration of their functionality, which leads to increased permeability of the cytoplasmic membrane [6–10].

Simple layered hydroxides (LHSs) are synthetic brucite-like structures that comprise hydroxylated layers with positive electrostatic charges stabilized by anions between layers, joined together by van der Waals forces [11]. Furthermore, they are promising materials owing to their properties like chemical and thermal stability, the ability to intercalate different types of anions (inorganic, organic, and biomolecules), sustained delivery of intercalated anions, and high biocompatibility [12]. Hybrid materials have proved to combine the properties of the LHS and the counter anion, sometimes a biomolecule, improving the solubility of hydrophobic compounds and increasing the systems in which they can be incorporated [12].

In this study, layered magnesium hydroxide compounds with thymol (LHS-Mg+T) and carvacrol (LHS-Mg+C) were synthesized through precipitation and ion exchange. X-ray diffraction (XRD), scanning electron microscopy (SEM), and Fourier transform infrared (FTIR) spectroscopy were employed to elucidate the composition and structure of the nanohydroxide; antioxidant activity was determined using the 2,2′-azinobis(3-ethylbenzothiazoline-6-sulfonic acid) (ABTS) technique, and antimicrobial activity was evaluated using the well diffusion technique, microdilution, and minimum inhibitory concentration (MIC) and minimum bactericidal concentration (MBC) against foodborne pathogens *E. coli*, *S. aureus*, *L. monocytogenes*, and *Salmonella* Enteritidis. Finally, the toxicity of hybrids was evaluated in the *Artemia salina* model.

2 Materials and methods

2.1 Materials

The magnesium LHS compounds with thymol (LHS-Mg+T) and carvacrol (LHS-Mg+C) were synthesized using $MgCl_2$ hexahydrate (FAGA LAB, Mexico), fructose 1% (Food Technologies Trading Co., Mexico), NaOH 0.1 M (Golden Bell Co., Mexico), thymol, and carvacrol (Sigma-Aldrich Inc., USA). Distilled water was used during the experimental period.

2.2 Synthesis of nanohydroxides and hybrids

The synthesis of magnesium nanohydroxides by precipitation (LHS-Mg) followed the methodology described by Wang et al. [13] with some modifications. Briefly, 0.04 g·mL^{-1} of $MgCl_2$ hexahydrate and 1% fructose as a reducing agent were dissolved in 100 mL of distilled water under constant stirring (IKA, Wilmington, USA) until the reagents were completely dissolved. Then, 0.1 M NaOH was added dropwise until a final pH of 11 and a white precipitate formed, allowing it to stabilize for 24 h at room temperature with constant stirring.

Subsequently, two washes with distilled water were performed by centrifugation (LZ-1580R, LaboGene, Yuseong-gu, South Korea) at 10,000 rpm for 10 min at 25°C. Finally, the precipitate was dried in a forced convection oven (FE-291, Felisa, Guadalajara, Mexico) at 40°C for 48 h and reserved until use.

To prepare the hybrid material with thymol and carvacrol, 50 mL of a solution of each compound was prepared at a concentration of 5 mg·mL^{-1}; then, 500 mg of LHS-Mg was added with constant stirring for 2 h. For the recovery of the precipitate, two washes were carried out under the conditions previously mentioned. Finally, the precipitate was dried in a forced convection oven at 40°C for 48 h and reserved until use [14].

2.3 Characterization

X-ray diffractograms were recorded in an Empyrean X-ray diffractor (Panalytical, Malvern, UK) using CuKα radiation at a 2θ angle between 5° and 70°, with a step of 0.02 and a collection time of 30 s. The analysis of the surface morphology of the nanohydroxides was carried out by SEM. The dried materials were placed in a sample holder overlaid with gold for 20 s; then, the micrographs were taken on a FE-SEM microscope (MIRA 3 LMU, TESCAN, Brno, Czech Republic) with an accelerating voltage of 15 kV. FTIR spectra were recorded in a spectrophotometer Cary 630 (Agilent Technologies, Santa Clara, USA) in absorbance mode in a wavenumber interval of 4,000–400 cm^{-1}, with 32 scans and 4 cm^{-1} of resolution [14].

2.4 Antioxidant activity

The antioxidant activity of hybrids was evaluated with the inhibition of the ABTS radical. The methodology reported

by Li et al. [15] with modifications was tested. Briefly, 280 µL of an ABTS solution previously adjusted to an absorbance of 0.7 at 750 nm was added to a 96-well microplate with 20 µL of solutions of the materials in ethanol (1:1 m/v). The plate was incubated for 15 min at room temperature in the dark. Then, absorbance was measured in a 96-well microplate reader (BioRad iMark™, CA, USA) at 750 nm; the percentage of inhibition was calculated with Eq. 1. Ethanol was used as negative control, while positive control was a solution of Trolox (50–400 µg·mL^{-1}) used for comparison:

$$\text{Inhibition (\%)} = \frac{[(A^0 - A^1)]}{A_0} \times 100 \quad (1)$$

where A^0 is the absorbance of the control and A^1 is the absorbance of the sample.

2.5 Antimicrobial evaluation

Simple bioactive compounds (thymol and carvacrol) and hybrid materials were evaluated against four bacterial strains: *E. coli* ATCC 8739, *S. aureus* ATCC 25923, *L. monocytogenes* (isolated from fresh cheese), and *Salmonella* Enteritidis from clinical cases. Bacteria were cultivated in Müller–Hinton broth (MHB) (DIFCO, USA) and incubated at 37°C for 18–24 h. Then, the concentration was adjusted to 1×10^8 cells·mL^{-1} with an optical density measured at 600 nm in a UV-Vis spectrophotometer (OPTIZEN, 131 Mecasys, South Korea).

Plate microdilution was performed in a 96-well microplate to determine the antimicrobial effect of LHS-Mg, bioactive compounds, and hybrids. Briefly, 160 µL of MHB was inoculated with 20 µL of 1×10^8 CFU·mL^{-1} of each strain, and then 20 µL of the bioactive compound, LHS, or hybrid at a concentration of 100 mg·mL^{-1} were added. Plates were incubated for 24 h at 37°C; PBS was used as a negative control, while 0.1% gentamicin (m/V) was a positive control. After incubation, plates were read at 600 nm in a BioRad microplate reader (BioRad, iMark™, CA, USA), and the percentage of inhibition was calculated with Eq. 2:

$$\%\ \text{reduction} = \frac{(A - B) \times 100}{A} \quad (2)$$

where A is the absorbance of the control and B is the absorbance of the treated compounds.

As for the well diffusion method, 100 µL (1×10^8 CFU·mL^{-1}) of the strains were inoculated by surface extension on Müller–Hinton agar (MHA); it was allowed to dry, and perforations were made with sterile tips (10 mm in diameter). Then, 60 µL of each bioactive compound and each hybrid material were placed. Finally, the plates were incubated for 24 h at 37°C, and the inhibition halos were measured. Positive and negative controls were the same as microdilution.

The MIC and MBC values were determined based on the methodology described by Gonçalves et al. [16] and the Clinical Laboratory Standards Institute [17]. The concentrations of the hybrid materials, thymol, and carvacrol, were determined using the methodology of Vasconcelos et al. [18] in 96-well microplates, with some modifications. Each well contained 160 µL of MHB, 20 µL of the inoculum (1×10^8 CFU·mL^{-1}), and 20 µL of standard or hybrid material with a 50–500 mg·mL^{-1} concentration. The microplates were incubated for 24 h at 37°C. Then, 30 µL of a 0.1 mg·mL^{-1} resazurin solution (Sigma-Aldrich, USA) was added to each well, and plates were incubated for 75 min at 37°C to observe the color change. Cell viability can be elucidated according to the color change of resazurin from blue to pink (resorufin). Serial dilutions were made for each well, and 100 µL was transferred to MHA with surface extension. After incubation with the same conditions previously used, colonies were counted. MIC was determined as the minimum concentration in which the inhibition was observed, while MBC was selected as the concentration where growth was absent.

2.6 Brine shrimp bioassay

In order to determine if hybrids exhibit cytotoxic effects, an evaluation with *Artemia salina* was conducted [19]. *A. salina* eggs were hatched in artificial seawater (34 g NaCl·L^{-1}) at 28°C with constant light and aeration for 24 h. Then, 10 nauplii were transferred to 6-well microplate with 5 mL of artificial seawater and 7 mm Whatman No. 4 filter papers wetted with LHS-Mg, LHS-Mg+T, or LHS-Mg+C solutions at different concentrations (50–200 mg·mL^{-1}). Hexane was used as the positive control. After 24 h, dead nauplii were counted, and the percentage of mortality was determined using Eq. 3:

$$\%M = \frac{N_m}{N_T} \times 100 \quad (3)$$

where N_m is the number of dead nauplii and N_T is the number of total nauplii at the beginning of the test. Toxicity was specified according to Clarkson criteria [20], and lethal dose (LD_{50}) was estimated with the PROBIT method [21] classifying the materials as non-toxic if LD_{50} > 1,000 µg·mL^{-1}, slightly toxic when 500 µg·mL^{-1} < LD_{50} < 1,000 µg·mL^{-1}, moderately toxic if 100 µg·mL^{-1} < LD_{50} < 500 µg·mL^{-1}, and extremely toxic when LD_{50} < 100 µg·mL^{-1}.

2.7 Statistical analysis

All the experiments were performed in triplicate (±SD), and the results were analyzed using ANOVA, followed by the Tukey HSD test with a p-value ≤ 0.05 using the Statgraphics Centurion (Statgraphics Centurion XVIII, version 18.1.12, USA) statistical program. In addition, illustrations were created using Origin 2022 (OriginLab Inc., USA).

3 Results and discussion

3.1 XRD analysis

Figure 1 depicts the XRD diffractogram for magnesium-layered hydroxide (LHS-Mg), thymol (LHS-Mg+T), and carvacrol (LHS-Mg+C) hybrids. All diffractogram peaks match the characteristics of brucite (ICDD Card No. 44-1482), demonstrating that brucite was obtained during the synthesis of LHS and hybrids [13]. Interestingly, the LHS-Mg+T diffractogram exhibits a first signal at 7.93° in the 2θ angle, which suggests a possible partial intercalation of thymol in the interlaminar space of the LHS due to the expansion of the space between layers according to Bragg's law [14]. Furthermore, the lower intensity peaks that appear in the range from 15° to 30° can be associated with diffraction peaks characteristic of thymol [22]. Both hybrids showed wider signals at each diffraction angle compared to LHS-Mg, indicating a reduction of particle crystallinity, possibly due to interactions of bioactive compounds on the surface of pristine compounds [23]. Also, the widening of the signal indicated as (001) is because of the substitution of water and OH^- in the interlaminar space for the biomolecules from the layered compound to the respective hybrids [24].

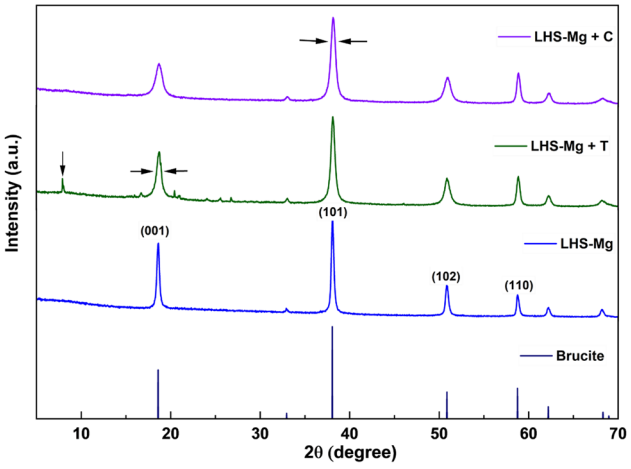

Figure 1: XRD diffractograms of LHS-Mg, LHS-Mg+T, and LHS-Mg+C.

3.2 SEM

Figure 2 depicts SEM micrography of LHS-Mg and hybrids. The characteristic hexagonal structure found in layered compounds was obtained for LHS-Mg (Figure 2a); small granules observed on the surface can also be attributed to the reducing agent. Reducing agents are added since it has been demonstrated that they control the growth rate of crystals, favoring the interaction between the crystal interphase and solvent [25]. Figure 2b shows an abundant formation of lamellar structures approximately 0.045 µm thick. In contrast, LHS-Mg+T and LHS-Mg+C produced larger size crystals, modifying their crystallinity as demonstrated by DRX analysis. Both terpenes formed a web-type structure around the brucite, similar to a coral (Figure 2c), which can result from the exposition of hydrophobic groups present in thymol and carvacrol molecules [26]. It is worth mentioning that substituting structural cations with other ions with less valence produces a charge deficiency on layers, which can be neutralized with adsorbed species located in the interlayer space [27]. When substituting anions in a layered compound, crystals grow in larger shapeless aggregates, as can be seen using positive ions such as copper [24].

3.3 FTIR analysis

FTIR spectra of brucite and hybrids are depicted in Figure 3. The signal around 3,700 cm^{-1} is associated with –OH vibrations, typical of LHS structures. In contrast, signals below 1,000 cm^{-1} can be attributed to metal bonds, confirming the formation of the brucite in the three materials. In the case of LHS-Mg+T, a small peak can be observed at around 2,900 cm^{-1}, a signal corresponding to a stretch of C–H bonds of the organic compound. Also, at around 1,430 cm^{-1}, thymol and carvacrol hybrids exhibit an arm compared to brucite alone, corresponding to C–H bonds [28,29].

3.4 Antimicrobial evaluation

The antibacterial activity of LHS-Mg, LHS-Mg+T, LHS-Mg +C, thymol, and carvacrol by microdilution was tested

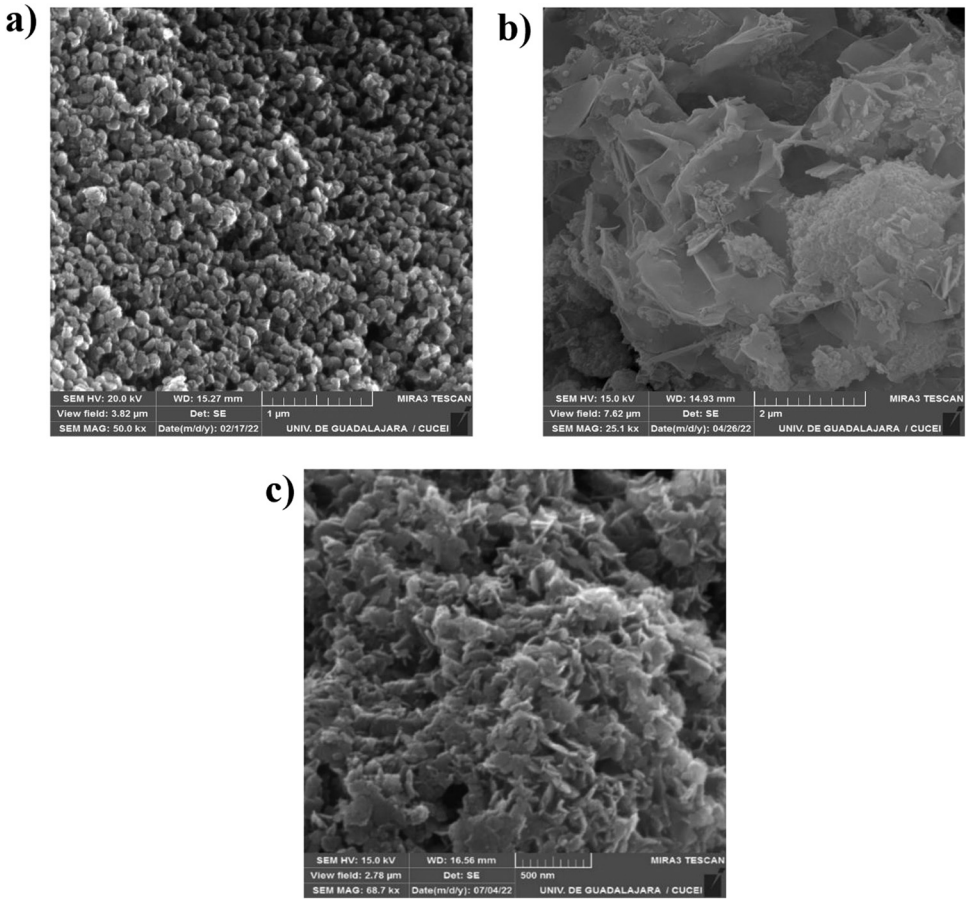

Figure 2: SEM micrographs of (a) LHS-Mg, (b) LHS-Mg+T, and (c) LHS-Mg+C.

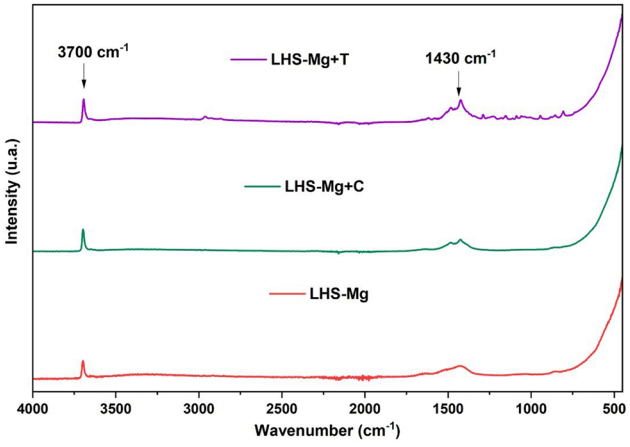

Figure 3: FT-IR spectra for LHS-Mg, LHS-Mg+T, and LHS-Mg+C.

against four foodborne pathogens. Figure 4 depicts the percentage of inhibition for each bacterial strain. The interaction of bioactive compounds with brucite is confirmed due to the increasing rate of inhibition of hybrids compared to the LHS alone. *E. coli* (Figure 4a) exhibited higher values of inhibition in comparison with gentamicin in both cases, while for *S. aureus* (Figure 4b) and *Salmonella* Enteritidis (Figure 4d), the increase exhibited for carvacrol in combination with brucite was significantly higher than when bioactive or brucite was used. However, the growth inhibition of *L. monocytogenes* (Figure 4c), although not significant, had a decrease in inhibition percentage. Similar results for *E. coli* and *S. aureus* were found by Clavier et al. [24] when exposing the bacterial strains to brucite nanoparticle solution at a concentration of 1 mg·mL^{-1}.

These results are in accordance with the ones obtained in the well diffusion test (Table 1), where inhibition halos increased for *E. coli, S. aureus,* and *Salmonella* Enteritidis. Carvacrol and LHS-Mg+C produced the same diameter with all strains, except *S. aureus*. However, in the case of *L. monocytogenes,* the diameter was higher for thymol and LHS-Mg +T than for LHS-Mg.

MIC values were not detected in the range of concentrations evaluated for bioactive compounds and hybrids, as shown in Table 2. MBC values were around 200 mg·mL^{-1} for bioactive compounds alone and hybrids but layered

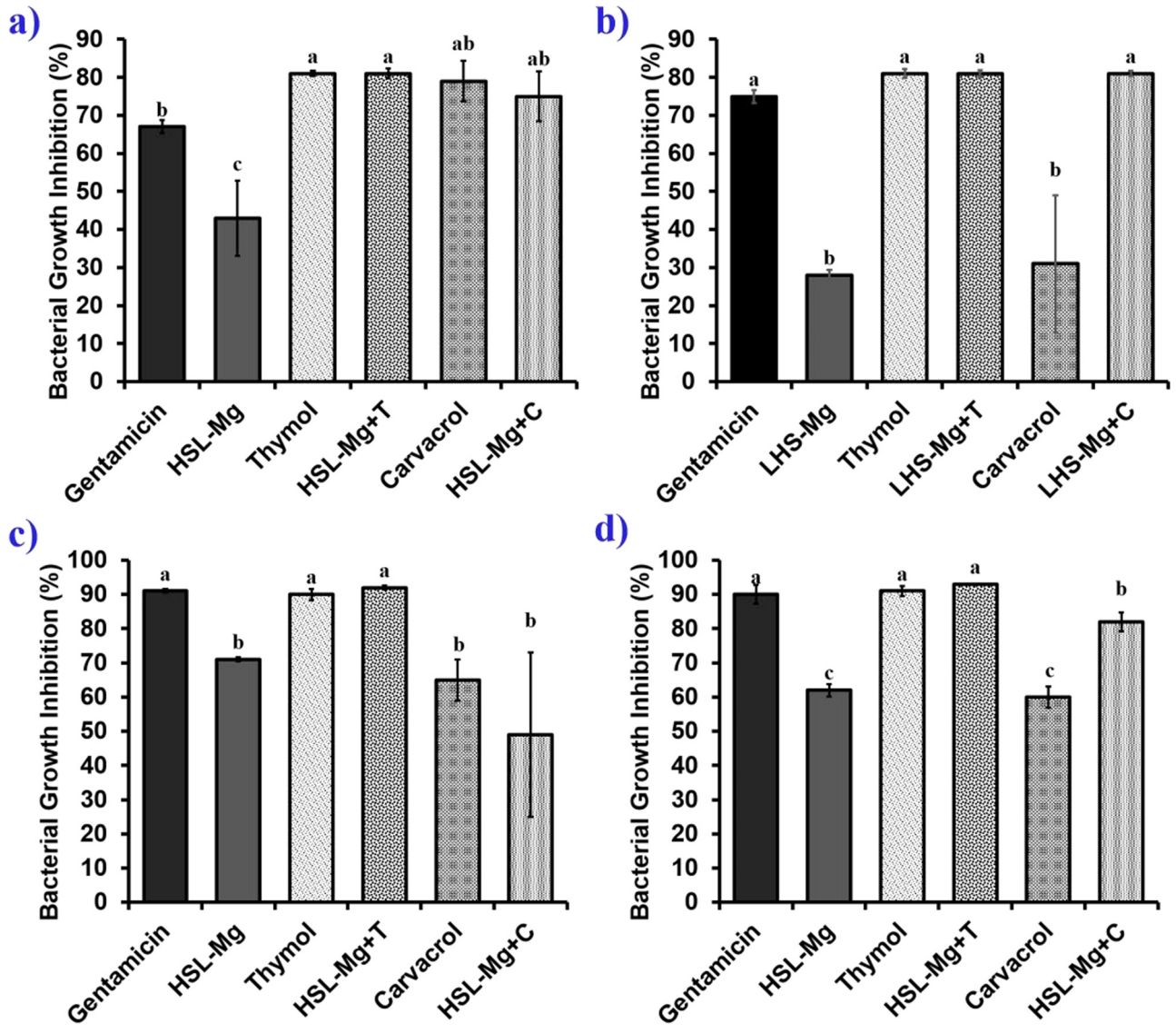

Figure 4: Bacterial growth inhibition of magnesium LHS, thymol, carvacrol, and hybrids. (a) *E. coli*, (b) *S. aureus*, (c) *L. monocytogenes*, and (d) *Salmonella* Enteritidis. Different letters indicate statistical differences ($p < 0.05$).

Table 1: Diameters of inhibition halos for bioactive compounds and hybrids

Material	Inhibition halo (mm)			
	E. coli	***S. aureus***	***L. monocytogenes***	***Salmonella* Enteritidis**
Gentamicin	17 ± 1.0^{c}	20 ± 2.5^{c}	20 ± 0.0^{b}	23 ± 1.2^{b}
LHS-Mg	15 ± 1.2^{cd}	14 ± 0.6^{d}	16 ± 2.0^{c}	12 ± 2.0^{c}
Thymol	23 ± 1.1^{b}	21 ± 1.2^{c}	25 ± 2.3^{a}	35 ± 5.0^{a}
LHS-Mg+T	49 ± 6.4^{a}	46 ± 1.1^{a}	27 ± 4.2^{a}	47 ± 9.9^{a}
Carvacrol	13 ± 1.0^{d}	15 ± 8.1^{cd}	14 ± 2.0^{cd}	15 ± 1.2^{c}
LHS-Mg+C	13 ± 1.2^{d}	35 ± 6.1^{b}	13 ± 1.2^{d}	15 ± 1.2^{c}

Results are mean ± SD from three replicates.
Different uppercase letters indicate statistical difference ($p < 0.05$).

Table 2: MIC and MBC for bioactive compounds and hybrids

Material	Concentration (mg·mL^{-1})							
	E. coli		*S. aureus*		*L. monocytogenes*		*Salmonella* Enteritidis	
	MIC	MBC	MIC	MBC	MIC	MBC	MIC	MBC
LHS-Mg	100	300	300	500	<50	300	250	500
Thymol	<50	200	<50	200	<50	200	<50	200
LHS-Mg+T	<50	200	<50	200	<50	>300	<50	200
Carvacrol	<50	200	<50	200	<50	200	<50	200
LHS-Mg+C	<50	200	<50	200	<50	>300	<50	>300

Results are mean ± SD from three replicates.
MIC: minimum inhibitory concentration.
MBC: minimum bactericidal concentration.

magnesium hydroxide reached values above 300 mg·mL^{-1}. At the same time, brucite exhibited values from 100 to 300 mg·mL^{-1} for some bacterial strains.

It has been proposed that magnesium nanoparticles can inhibit bacterial growth due to OH^- radicals interacting with the cell membrane, increasing its pH and provoking cell death [30]. Depending on whether the bacteria are Gram-positive or -negative, this mechanism may vary since, in the latter, the presence of lipopolysaccharides may limit the diffusion of hydrophobic compounds [31]. Other mechanisms through which layered compounds exhibit antibacterial activity are due to the formation of reactive oxygen species (ROS), superoxide ions, or hydrogen peroxide, which can oxidize the lipid membrane and favor cellular content leakage, altering metabolic processes and provoking cell death [32].

The size and surface charge of nanoparticles also play a crucial role in antibacterial activity. Magnesium nanosheets may interact with bacterial cells attaching to the cell membrane and then integrating inside the cell, destroying and inactivating the cell wall [33]. Bioactive compounds like thymol and carvacrol interact with the cell membrane, generating pores and leading to cell content leakage [34]. Modifying the surface of layered compounds has been demonstrated to increase the antimicrobial activity of these materials. It has been proved that functionalizing magnesium LHSs with poly (sodium 4-styrene sulfonate) or poly(allylamine hydrochloride) increases the inhibition of microorganisms like *E. coli* or *S. cerevisiae* since the combination of materials improves the attachment to cell walls, promoting its disruption and, in consequence, cell death [35,36]. Brucite structure has been used as a host for the anti-tuberculosis antibiotic pyrazinamide (PZA) and tested against *E. coli, S. aureus*, and *M. tuberculosis*, where activity was upgraded compared to independent hydroxide salt or PZA [37]. The combination of brucite and bioactive compounds may act, generating holes in the membrane and favoring the introduction of magnesium ions and OH^- groups, which can explain the elevation of inhibition percentage and diameter of the inhibition halo.

3.5 Antioxidant activity

Table 3 shows the percentage of inhibition of the ABTS radical for LHS-Mg, LHS-Mg+T, LHS-Mg+C, thymol, and carvacrol. ABTS inhibition for carvacrol increased when the hybrid was evaluated from 16 to 65%, while thymol activity decreased from 93 to 80%. Comparing these results with the antioxidant activity of Trolox (data not shown), it can be seen that LHS-Mg and LHS-Mg+C activity exhibits the same percentage of ABTS radical inhibition of 250 μg·mL^{-1}, carvacrol as 40 μg·mL^{-1}, LHS-Mg+T for 300 μg·mL^{-1}, and thymol as 400 μg·mL^{-1} of Trolox. The ABTS inhibition of thymol intercalated in the layered zinc hydroxide has been previously evaluated, demonstrating that hybrids exhibit slightly higher inhibition [14], in which thymol was mainly on the surface of the nanoparticle. In this work, a fraction of thymol was intercalated inside the brucite structure as suggested by XRD, which affects the

Table 3: Antioxidant activities of bioactive compounds and hybrids

Material	ABTS inhibition (%)	Trolox equivalent (μg·mL^{-1})*
LHS-Mg	60 ± 7.5	250
Thymol	93 ± 0.1	400
LHS-Mg+T	80 ± 2.0	300
Carvacrol	16 ± 5.5	40
LHS-Mg+C	65 ± 2.1	250

Results are mean ± SD from three replicates.
*Data obtained from the standard curve (not shown).

Table 4: Cytotoxic activities and LD_{50} values estimated using the PROBIT test of hybrids

Material	Mortality (%)				PROBIT
	Concentration ($mg \cdot mL^{-1}$)				LD_{50} ($mg \cdot mL^{-1}$)
	25	50	100	200	
Hexane	70 ± 0.0	70 ± 0.0	70 ± 0.0	70 ± 0.0	
LHS-Mg	0.0 ± 0.0	0.0 ± 0.0	0.0 ± 0.0	10 ± 14	19
LHS-Mg+T	0.0 ± 0.0	0.0 ± 0.0	0.0 ± 0.0	5.0 ± 7.1	165
LHS-Mg+C	0.0 ± 0.0	0.0 ± 0.0	0.0 ± 0.0	10 ± 14	1,008

Results are mean ± SD from three replicates.

activity of this radical inhibition in the concentration evaluated. Conversely, as shown by the SEM and XRD results, carvacrol is located on the surface. Its activity was increased in combination with brucite, probably due to ROS production [8].

3.6 *Artemia salina* bioassay

The nauplii of *Artemia salina* were mixed with LHS-Mg, LHS-Mg+T, and LHS-Mg+C in the concentration range from 25 to 200 $mg \cdot mL^{-1}$. After 24 h, results demonstrated that all materials were non-toxic according to the Clarkson scale [20] since the mortality percentage was up to 10% (Table 4). The LD_{50} calculated with the PROBIT test indicated that a high dose of the materials is required to cause multiple nauplii deaths, corroborating that these materials are nontoxic (Table 4). Thymol and carvacrol are molecules that have OH^- radicals in their structure; at high concentrations, these radicals may exhibit a lethal effect on *Artemia salina* nauplii and even on human cells [38], but the bioavailability of these bioactive compounds can be controlled since they interact with the nanohydroxide structure. In the case of magnesium nanoparticles obtained from different precursors, it has been demonstrated that they are safe to be in contact with human cells at concentrations of 1,000 $\mu g \cdot mL^{-1}$ [39], as nitrate is the counter ion that exhibits a slight cytotoxic effect for the pristine LHS [37]. These results suggest that the synthesized and evaluated hybrids are safe for their application in food matrices, reducing the growth of pathogens and exhibiting antioxidant activity.

4 Conclusions

Hybrids of magnesium-LHS with thymol or carvacrol were obtained, whose structures were confirmed with solid-state techniques. Antibacterial activity against foodborne pathogens suggests that these hybrids can be incorporated in food matrices or applied as disinfectants to control the proliferation of microorganisms since they proved innocuous on *Artemia salina* nauplii. The results obtained from this research open a new path to introduce layered magnesium compounds to stabilize and potentiate the antioxidant and antimicrobial activity of terpenes such as thymol and carvacrol, keeping in mind that the safety of consumers is a priority in food research.

Acknowledgments: This research was supported by the Council of Humanities, Science and Technology CONAHCyT (Grant number 1100443) and the University of Guadalajara.

Author contributions: Castorena-Sánchez: methodology, formal analysis, investigation, and writing-original draft. Velázquez-Carriles: methodology, formal analysis, writing-original draft, and investigation. López-Álvarez: resources and data curation. Serrano-Niño: resources and supervision. Cavazos-Garduño: data curation and conceptualization. Garay-Martínez: data curation and formal analysis. Silva-Jara: project administration, resources, investigation, visualization, writing-original draft, formal analysis, and software.

Conflict of interest: The authors state no conflict of interest.

Data availability statement: The datasets generated during and/or analyzed during the current study are available from the corresponding author on reasonable request.

References

[1] Administración Nacional de Medicamentos, Alimentos y Tecnología Médica (ANMAT). Enfermedades Transmitidas por Alimentos. 2021. Retrieved from http://www.anmat.gov.ar/alimentos/eta.pdfAccessed 12, November 2021.

[2] World Health Organization (WHO). Food safety. 2020 Apr. Retrieved from https://www.who.int/es/news-room/fact-sheets/detail/food-safetyAccessed 18, November 2021.

[3] Centers for Disease Control and Prevention (CDC). Foodborne Germs and Illnesses. 2021. Retrieved from https://www.cdc.gov/foodsafety/es/foodborne-germs-es.htmlAccessed 12, November 2021.

[4] Soto-Varela Z, Pérez-Lavalle L, Estrada-Alvarado D. Bacterias causantes de enfermedades transmitidas por alimentos: Una mirada en Colombia. Sal Uninor. 2016;32(1):105–22. doi: 10.14482/sun.32.1.8598.

[5] Abdelhamid GA, El-Dougdoug KN. Controlling foodborne pathogens with natural antimicrobials by biological control and

antivirulence strategies. Heliyon. 2020;6(9):2–7. doi: 10.1016/j.heliyon.2020.e05020.
[6] Pisoschi AM, Pop A, Georgescu C, Turcuş V, Kinga ON, Mathe E. An overview of natural antimicrobials role in food. Eur J Med Chem. 2018;143(1):922–35. doi: 10.1016/j.ejmech.2017.11.095.
[7] Kachur K, Suntres Z. The antibacterial properties of phenolic isomers, carvacrol and thymol. Crit Rev Food Sci Nutr. 2019;60(18):3042–53. doi: 10.1080/10408398.2019.1675585.
[8] Rúa J, Del Valle P, De Arriaga D, Fernández-Álvarez L, García-Armesto MR. Combination of carvacrol and thymol: Antimicrobial activity against *Staphylococcus aureus* and antioxidant activity. Foodborne Pathog Dis. 2019;16(9):622–9. doi: 10.1089/fpd.2018.2594.
[9] Sivaranjani D, Saranraj P, Manigandan M, Amala K. Antimicrobial activity of *Plectranthus amboinicus* solvent extracts against Human Pathogenic Bacteria and Fungi. J Drug Deliv Ther. 2019;9(3):36–9. doi: 10.22270/jddt.v9i3.2604.
[10] Soumya E, Saad KI, Hassan L, Ghinzlane Z, Hind M, Adnane R. Carvacrol and thymol components inhibiting *Pseudomonas aeruginosa* adherence and biofilm formation. Afr J Microbiol Res. 2011;5(20):3229–32. doi: 10.5897/AJMR11.275.
[11] Martínez RD, Carbajal GG. Hidróxidos dobles laminares: arcillas sintéticas con aplicaciones en la nanotecnología. Av en Química. 2012;7(1):87–99.
[12] Mishra G, Dash B, Pandey S. Layered double hydroxides: A brief review from fundamentals to application as evolving biomaterials. Appl Clay Sci. 2018;153:172–86. doi: 10.1016/j.clay.2017.12.021.
[13] Wang X, Yu M, Li L, Fan X. Synthesis and morphology control of nano-scaled magnesium hydroxide and its influence on the mechanical property and flame retardancy of polyvinyl alcohol. Mater Express. 2019;9(6):675–80. doi: 10.1166/mex.2019.1545.
[14] Velázquez-Carriles C, Macías-Rodríguez ME, Ramírez-Alvarado O, Corona-González RI, Macias-Lamas A, García-Vera I, et al. Nanohybrid of thymol and 2D simonkolleite enhances inhibition of bacterial growth, biofilm formation, and free radicals. Molecules. 2020;27(19):6161. doi: 10.3390/molecules27196161.
[15] Li H, Wang X, Li P, Li Y, Wang H. Comparative study of antioxidant activity of grape (*Vitis vinifera*) seed powder assessed by different methods. J Food Drug Anal. 2008;16(6):67–73. doi: 10.38212/2224-6614.2321.
[16] Gonçalves TB, Braga MA, de Oliveira FFM, Santiago GMP, Carvalho CBM, Cabral PB, et al. Effect of subinihibitory and inhibitory concentrations of *Plectranthus amboinicus* (Lour.) Spreng essential oil on *Klebsiella pneumoniae*. Phytomedicine. 2012;19(11):962–8. doi: 10.1016/j.phymed.2012.05.013.
[17] Clinical and Laboratory Standards Institute (CLSI). Methods for dilution antimicrobial susceptibility test for bacteria that grow aerobically; approved standard. 2012. Retrieved from https://www.researchgate.net/file.PostFileLoader.html?id=564ceedf5e9d97daf08b45a2&assetKe y=AS%3A297254750572544%401447882463055Accessed 15, November 2021.
[18] Vasconcelos SECB, Melo HM, Calvacante TTA, Júnior FEAC, de Carvalho MG, Menezes FGR, et al. *Plectranthus amboinicus* essential oil and carvacrol bioactive against planktonic and biofilm of oxacillin- and vancomycin-resistant *Staphylococcus aureus*. BMC Complement Altern Med. 2017;17(1):2–9. doi: 10.1186/s12906-017-1968-9.
[19] Casas-Junco PP, Solís-Pacheco JR, Ragazzo-Sánchez JA, Aguilar-Uscanga BR, Bautista-Rosales PU, Calderón-Santoyo M. Cold plasma treatment as an alternative for ochratoxin a detoxification and inhibition of mycotoxigenic fungi in roasted coffee. Toxins. 2019;11(6):337. doi: 10.3390/toxins11060337.
[20] Clarkson C, Maharaj VJ, Crouch NR, Grace OM, Pillay P, Matsabisa MG, et al. *In vitro* antiplasmodical activity of medicinal plants native to or naturalized in South Africa. J Ethnopharmacol. 2004;92(2–3):177–91. doi: 10.1016/j.jep.2004.02.011.
[21] Ates M, Daniels J, Arslan Z, Farah IO. Effects of aqueous suspensions of titanium dioxide nanoparticles on *Artemia salina*: assessment of nanoparticle aggregation, accumulation, and toxicity. Environ Monit Assess. 2013;185(4):3339–48. doi: 10.1007/s10661-012-2794-7.
[22] Trivedi MK, Patil S, Mishra RK, Jana S. Structural and physical properties of biofield treated thymol and menthol. J Mol Pharm Org Process Res. 2015;3(2):1000127. doi: 10.4172/2329-9053.1000127.
[23] Sierra-Fernández A, Gómez-Villalba LS, Muñoz L, Flores G, Fort R, Rabanal ME. Effect of temperature and reaction time on the synthesis of nanocrystalline brucite. Int J Mod Manuf Technol. 2014;6(1):50–4.
[24] Clavier B, Baptiste T, Massuyeau F, Jounanneaux A, Guiet A, Boucher F, et al. Enhanced bactericidal activity of brucite through partial copper substitution. J Mater Chem B. 2020;8:100–13. doi: 10.1039/C9TB01927H.
[25] Liu Z, Yang Y, Fan W, Yu H, Zhang W, Zhong H, et al. Hydro thermal synthesis and morphology control of magnesium hydroxide flame retardant. Chem World. 2002;11:612–4. doi: 10.1166/mex.2019.1545.
[26] Hidouri S, Jafari R, Fournier C, Girard C, Momen G. Formulation of nanohybrid coating based on essential oil and fluoroalkyl silane for antibacterial superhydrophobic surfaces. Appl Surf Sci Adv. 2022;9:100252. doi: 10.1016/j.apsadv.2022.100252.
[27] Constantino-Vera RI, Barbosa CAS, Bizeto MA, Dias PM. Intercalation compounds involving inorganic layered structures. An Acad Bras Ciénc. 2000;72(1):45–9. doi: 10.1590/s0001-37652000000100006.
[28] Ziyat H, Naciri Bennani M, Hajjaj H, Mekdad S, Qabaquos O. Synthesis and characterization of crude hydrotalcite Mg–Al–CO_3: Study of thymol adsorption. Res Chem Intermed. 2018;44:4163–77. doi: 10.1007/s11164-018-3361-9.
[29] Tian Q, Yin WZ, Zhang LL, Liu L. Synthesis of hydrotalcite using brucite as the source of magnesium. Adv Mater Res. 2010;158:241–7. doi: 10.4028/www.scientific.net/AMR.158.241.
[30] Dong C, He G, Zheng W, Bian T, Li M, Zhang D. Study on antibacterial mechanism of $Mg(OH)_2$ nanoparticles. Mater Lett. 2014;134(1):286–9. doi: 10.1016/j.matlet.2014.07.110.
[31] Shrivastava R, Chng SS. Lipid trafficking across the Gram-negative cell envelope. J Biol Chem. 2019;294(39):14175–84. doi: 10.1074/jbc.AW119.008139.
[32] Zhu Y, Tang Y, Ruan Z, Dai Y, Li Z, Lin Z, et al. $Mg(OH)_2$ nanoparticles enhace the antibacterial activities of macrophages by activating the reactive oxygen species. J Biomed Mater Res. 2021;19(11):23692380. doi: 10.1002/jbm.a.37219.
[33] Pan X, Wang Y, Chen Z, Pan D, Chen Y, Liu Z, et al. Investigation of antibacterial activity and related mechanism of a series of Nano-$Mg(OH)_2$. ACS Appl Mater Interfaces. 2014;5(3):1137–42. doi: 10.1021/am302910q.
[34] Kim H, Lee S, Son B, Jeon J, Kim D, Lee W, et al. Biocidal effect of thymol and carvacrol on aquatic organisms: Possible application in ballast water management systems. Mar Pollut Bull. 2018;133:734–40. doi: 10.1016/j.marpolbul.2018.06.025.
[35] Halus AF, Horozov TS, Paunov VN. Controlling the antimicrobial action of surface modified magnesium hydroxide

nanoparticles. Biomimetics. 2019;4(2):41. doi: 10.3390/biomimetics4020041.

[36] Saifullah V, Arulselvan P, El-Zowalaty ME, Tan WS, Fakurazi P, Webster TJ, et al. A novel para-amino salicylic acid magnesium layered hydroxide nanocomposite anti-tuberculosis drug delivery system with enhanced *in vitro* therapeutic and antiinflammatory properties. Int J Nanomedicine. 2021;16:7035–50. doi: 10.2147/IJN.S297040.

[37] Saifullah B, Arulselvan P, Fakurazi S, Webster TJ, Bullo N, Hussein MZ, et al. Development of a novel anti-tuberculosis nanodelivery formulation using magnesium layered hydroxide as the nanocarrier and pyrazinamide as a model drug. Sci Rep. 2022;12:14086. doi: 10.1038/s41598-022-15953-6.

[38] Kimbaris AC, González-Coloma A, Andrés MF, Vidali VP, Polissiou MG, SantanaMéridas O. Biocidal Compounds from *Mentha* sp. Essential Oils and Their Structure-Activity Relationships. Chem Biodivers. 2017;14(3):1–13. doi: 10.1002/cbdv.201600270.

[39] Alves MM, Batista C, Mil-Homens D, Grenho L, Fernandes MH, Santos CF. Enhanced antibacterial activity of Rosehip extract-functionalized $Mg(OH)_2$ nanoparticles: An *in vitro* and *in vivo* study. Colloids Surf B: Biointerfaces. 2022;217:112643. doi: 10.1016/j.colsurfb.2022.112643.